ACS OMEGA

http://pubs.acs.org/journal/acsodf Article

Synthesis and Characterization of a Trigonal Layered Compound $AgInS_2$

Takahiro Sawahara, Ryo Matsumoto, Yuki Nakahira, Hidetomo Usui, Noriyuki Kataoka, Ryusei Saitou, Takanori Wakita, Takayoshi Yokoya, Aichi Yamashita, Yosuke Goto, Yoshihiko Takano, Akira Miura, and Yoshikazu Mizuguchi*

Cite This: ACS Omega 2023, 8, 11288–11292

ABSTRACT: Depending on thermal and pressure conditions, $AgInS_2$ exhibits various crystal structures. In this study, we synthesized a high-purity polycrystalline sample of trigonal $AgInS_2$, which is a layered compound, using a high-pressure synthesis technique. The crystal structure was investigated by synchrotron powder X-ray diffraction and the Rietveld refinement. On the basis of band calculation, X-ray photoelectron spectroscopy, and electrical resistance measurements, we found that the obtained trigonal $AgInS_2$ is a semiconductor. Temperature dependencies of electrical resistance of $AgInS_2$ were measured by a diamond anvil cell up to 31.2 GPa. Although semiconducting behavior was suppressed with pressure, metallic behavior was not observed within the pressure range investigated in this study.

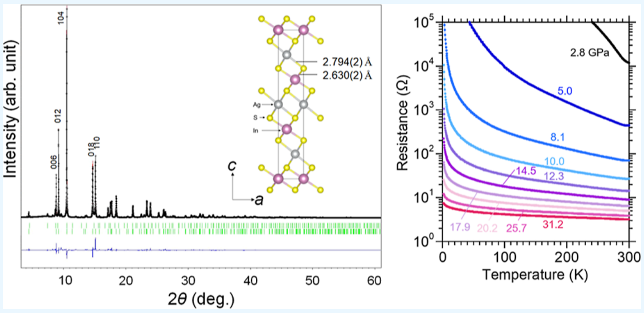

1. INTRODUCTION

I–III–VI ternary semiconductor compounds, such as $AgInS_2$, $AgGaS_2$, $CuGaTe_2$, etc., have been extensively studied due to various notable structural, electrical, and optical properties and their advantages for the use in solar cells, thermoelectric materials, photosensitizers, and optical devices.[1−9] Among them, $AgInS_2$ is an interesting compound that shows various crystal structures depending on thermal and pressure conditions. $AgInS_2$ presents as three types as shown in Figure 1. Under ambient pressure, the structure at high temperatures is orthorhombic (space group: $Pna2_1$, no. 33), and it changes to tetragonal (space group: $I\bar{4}2d$, no. 122) at low temperatures. This phase transition from orthorhombic to tetragonal occurs at 893 K.[10,11] Furthermore, the crystal structure changes to trigonal (space group: $R\bar{3}m$, no. 166) under high pressures; a theoretical study suggested that a trigonal phase is present above 1.78 GPa.[12] The electronic structure has been investigated theoretically for several types of $AgInS_2$.[13,14] However, there are almost no synthesis reports on $AgInS_2$ with the trigonal phase.

We aimed to study the crystal structure and physical properties of trigonal $AgInS_2$ because it is a layered compound, which consists of InS_2 layers connected with Ag ions. As is well-known, intercalation/deintercalation and substitution of the interlayer ions in such layered compounds (chalcogenides) modify the physical properties. Notably, superconductivity has been observed in these layered chalcogenides, such as Na_xTaS_2, Cu_xTiSe_2, Cu_xPdTe_2, and $SnTaS_2$.[15−18] Furthermore, pressure-induced superconductivity was reported for similar layered compounds like $PbBi_2Te_4$ and $SnBi_2Se_4$.[19,20] Those phases are semiconductors under ambient pressure, but they exhibit metallic behavior and superconductivity under high pressures. Therefore, synthesizing new semiconducting layered chalcogenides and testing pressure effects could be a potential way to open a new research field on superconductivity. Here, we synthesized a high-purity polycrystalline sample of trigonal $AgInS_2$ using high-pressure synthesis and investigated its structural, electronic, and physical properties including resistance under high pressures.

2. METHODS

Polycrystalline samples of $AgInS_2$ were prepared by high-pressure synthesis with a starting composition of Ag_xInS_2 because a slight reduction of the Ag amount in the starting composition resulted in high-purity samples. Powders and grains of Ag (99.9%), S (99.9999%), and In_2S_3 (99.99%) with $x = 0.9$ were mixed and pelletized into a pellet with a diameter of 5 mm. The pellet was set in a high-pressure cell, which is composed of a BN sample capsule, a carbon heater capsule,

Received: December 31, 2022
Accepted: March 6, 2023
Published: March 16, 2023

https://doi.org/10.1021/acsomega.2c08289
ACS Omega 2023, 8, 11288–11292

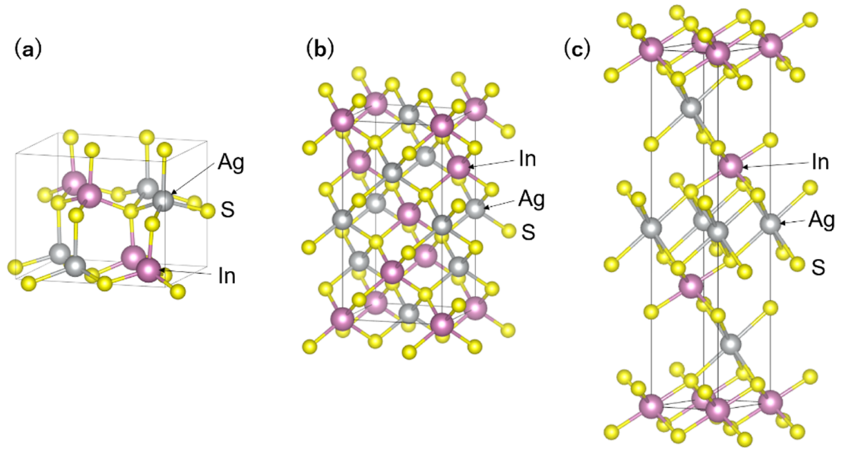

Figure 1. Schematic images of the crystal structure of (a) orthorhombic. (b) tetragonal, and (c) trigonal phases. The solid lines indicate unit cells. The schematic images were drawn using VESTA.

electrodes, and a pyrophyllite cubic cell. We used a cubic anvil-type 180 ton press to pressurize; pressing from six directions can generate isotropic pressures to the cell. The load was controlled within ±0.2 ton during the synthesis. By applying DC current to the carbon capsule, temperature of the inner sample was controlled, and the resulting temperature was corrected by the data taken with the thermocouple. The high-pressure synthesis condition was optimized by repeating synthesis with different pressure (P) and temperature (T) conditions, and we finally obtained the optimal condition of P = 3 GPa and T = 873 K for 30 min. See the Supporting Information (Figures S1−S3) for the X-ray diffraction (XRD) patterns of various samples prepared under different conditions.

The phase purity and crystal structure of the obtained sample were examined by synchrotron powder X-ray diffraction (SPXRD) performed at the BL02B2 beamline of SPring-8 (proposal no.: 2021B1175). The wavelength of the synchrotron X-ray was 0.496118(1) Å. The diffraction data were collected at T = 293 K and ambient pressure using a high-resolution semiconductor detector (multiple MYTHEN system) with a scanning step of $2\theta \sim 0.006$ deg.[21] The crystal structure parameters were refined by the Rietveld method using the Jana2020 software.[22] The schematic images shown in this article were drawn using the VESTA software.[23] The atomic ratio of the obtained sample was investigated by an energy-dispersive X-ray spectroscopy (EDX) using Oxford, SwiftED3000 on a scanning electron microscope using Hitachi, TM3030. The average composition was $Ag_{0.72(4)}In_{0.95(2)}S_2$: the amount of S was fixed as 2, and the errors (standard deviations) were determined from six data points.

The first principles band calculations were performed using the experimentally determined crystal structure shown in Table 1. The full-potential linearized augmented plane-wave method was used as implemented in the WIEN2K package.[24] The electronic density was calculated self-consistently with the Perdew−Burke−Ernzerhof generalized gradient approximation exchange−correlation functional.[25] The k-mesh and RK_{max} were set to 10 × 10 × 10 and 7, respectively.

The temperature dependence of electrical resistance under high pressure was measured by a diamond anvil cell (DAC) with boron-doped diamond electrodes. The details of the DAC experiments performed here are described in ref 26. As a pressure-transmitting medium, cubic boron nitride powder with a ruby manometer was used. Applied pressure was estimated by the fluorescence from the ruby powders and by the Raman spectrum from the culet of the top diamond anvil using an inVia Raman microscope (RENISHAW).

Table 1. Structural Parameters of $AgInS_2$ Determined by Rietveld Refinement

phase	$AgInS_2$
space group	trigonal $R\overline{3}m$ (no. 166)
a (Å)	3.77188(2)
c (Å)	19.3494(2)
Ag (x, y, z)	(0, 0, 0.5)
In (x, y, z)	(0, 0, 0)
S (x, y, z)	(0, 0, 0.25712(13))
U_{iso} (Ag) (Å^2)	0.0188(5)
U_{iso} (In) (Å^2)	0.0152(4)
U_{iso} (S) (Å^2)	0.0081(4)
R_{wp}	7.8%

3. RESULTS AND DISCUSSION

The average composition of the obtained sample was $Ag_{0.72(4)}In_{0.95(2)}S_2$. Although the Ag site is not close to 1, we consider that the deviation from the nominal composition is due to the presence of the minor impurity phase of $AgIn_5S_8$. The crystal structure and phase purity were investigated by the Rietveld refinements. Figure 2 shows the SPXRD pattern and the Rietveld refinement result for $AgInS_2$. Almost all the peaks were assigned to those of trigonal $AgInS_2$. We found, however, a minor impurity phase of $AgIn_5S_8$. The weight ratios determined by the refinement are 91.7 wt % for $AgInS_2$ and 8.3 wt % for $AgIn_5S_8$. Since the $AgIn_5S_8$ phase is a wider-gap semiconductor with a gap greater than 2 eV,[27] we assumed that the present transport results are not affected by the presence of 8.3% impurity of $AgIn_5S_8$. The structural parameters determined by the refinement are summarized in Table 1. As shown in the inset of Figure 2, the bond length of the In−S bond (2.630(2) Å) is shorter than that of the Ag−S bond (2.794(2) Å), which is due to the different ionic radius of Ag^+ (115 pm) and In^{3+} (80 pm).[28]

Using the obtained crystal structure parameters, we calculated the electronic structure of trigonal $AgInS_2$ (Figure 3). There is a band gap with a size of ∼0.14 eV. The orbitals near Fermi energy (E_F) are contributed by the Ag and S

https://doi.org/10.1021/acsomega.2c08289
ACS Omega 2023, 8, 11288−11292

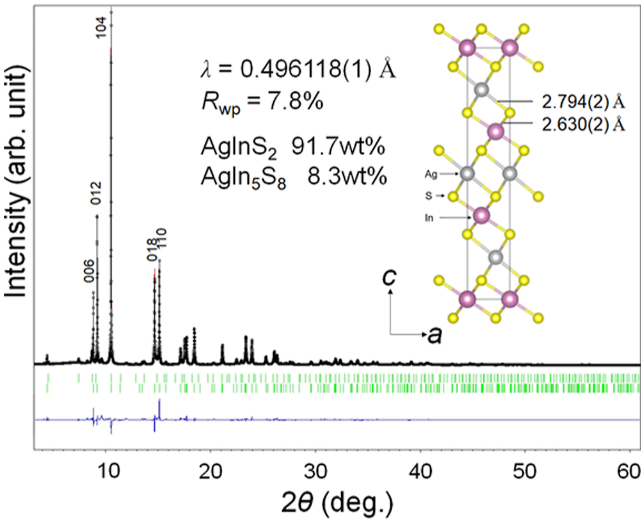

Figure 2. SPXRD pattern taken at T = 293 K and ambient pressure and Rietveld refinement result for $AgInS_2$. The green vertical marks indicate the Bragg diffraction positions for $AgInS_2$ (lower one) and $AgIn_5S_8$ (upper one). The difference between observed and calculated intensities is shown at the bottom. The numbers in the figure indicate Miller indices for major peaks of the $AgInS_2$ phase. The inset shows a schematic image of the refined structure with the bond lengths of In−S and Ag−S.

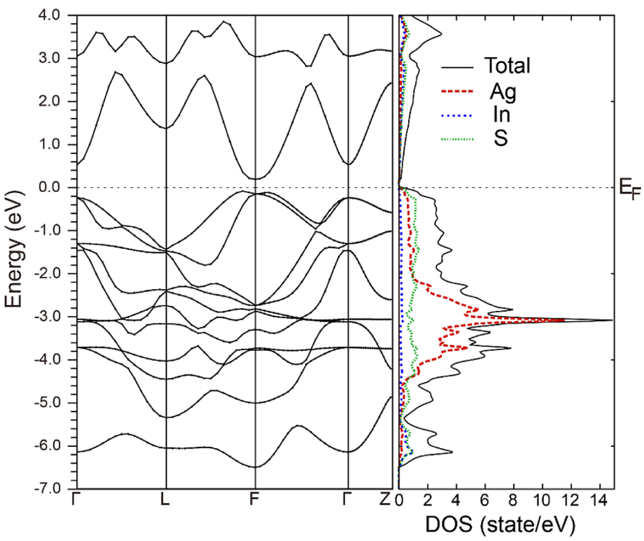

Figure 3. Electronic band structure of trigonal $AgInS_2$.

orbitals. We confirmed the valence state of In to be In^{3+} by the core-level spectrum (see Supporting Information, Figure S4), where the presence of In^{+} is eliminated for $AgInS_2$. Furthermore, we can simply conclude that the valence state of Ag is in Ag^{+} on the basis of the semiconducting electronic structure of $AgInS_2$.

To investigate further physical properties, we measured the electrical resistance of $AgInS_2$ by the DAC. Figure 4 shows the temperature dependences of electrical resistance under various pressures ranging from 2.8 to 31.2 GPa. The resistance at low pressure is quite high, which suggests the absence of mobile carriers. On the basis of the valence states examined above, we consider that there are almost no defects for all the sites because mobile holes should be generated with defects of cations, Ag^{+} and/or In^{3+}. We must mention another possibility

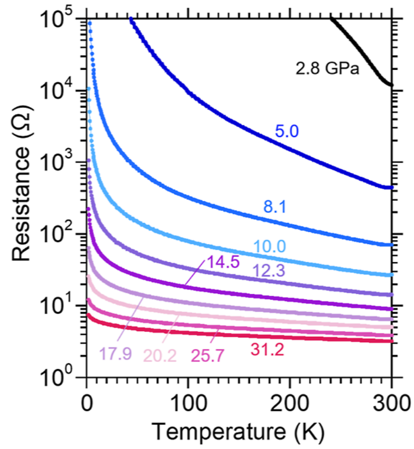

Figure 4. Temperature and pressure dependence of electrical resistance for $Ag_{0.9}InS_2$.

of carrier compensation by both defects of both cations and anions. With pressure, the values of resistance tend to decrease, but metallic conductivity was not observed within the pressure range examined here. Although we expected superconductivity under pressures, no signal of superconductivity was observed under pressures below 31.2 GPa. Generally, pressure-induced superconductivity in a semiconductor is observed when the transport properties exhibited (almost) metallic behavior.[19] To induce metallic conductivity, a higher pressure should be applied; at the metallic phase, we may observe superconductivity.

4. SUMMARY

Motivated by the extensive exploration of functional materials including superconductors in I−III−VI ternary semiconductor compounds and doped phases, we synthesized a high-pressure phase of $AgInS_2$ by a high-pressure synthesis method and confirmed the crystal structure to be trigonal. The electronic structure was examined by band calculations and the core-level spectrum. Trigonal $AgInS_2$ is a semiconductor with a band gap of ∼0.14 eV, and the valence states of cations are Ag^{+} and In^{3+}. We measured electrical resistance under pressures up to 31.2 GPa, but the pressures were not enough to induce metallicity in the compound. No superconductivity was observed in trigonal $AgInS_2$ under pressure..

■ ASSOCIATED CONTENT

Supporting Information

The Supporting Information is available free of charge at https://pubs.acs.org/doi/10.1021/acsomega.2c08289.

XRD patterns for samples synthesized for the optimization of synthesis conditions and the In valence state studied by spectroscopy (PDF)

■ AUTHOR INFORMATION

Corresponding Author

Yoshikazu Mizuguchi − *Department of Physics, Tokyo Metropolitan University, Hachioji, Tokyo 192-0397, Japan;* orcid.org/0000-0002-4771-7805; Email: mizugu@tmu.ac.jp

Authors

Takahiro Sawahara − *Department of Physics, Tokyo Metropolitan University, Hachioji, Tokyo 192-0397, Japan*

https://doi.org/10.1021/acsomega.2c08289
ACS Omega 2023, 8, 11288−11292

Ryo Matsumoto − *International Center for Materials Nanoarchitectonics (MANA), National Institute for Materials Science, Tsukuba, Ibaraki 305-0047, Japan;* orcid.org/0000-0001-6294-5403
Yuki Nakahira − *Quantum Beam Science Research Directorate, National Institutes for Quantum Science and Technology, Sayo-cho, Hyogo 679-5148, Japan;* orcid.org/0000-0003-0241-0786
Hidetomo Usui − *Department of Physics and Materials Science, Shimane University, Matsue 690-8504, Japan*
Noriyuki Kataoka − *Graduate School of Natural Science and Technology, Okayama University, Okayama 700-8530, Japan*
Ryusei Saitou − *Graduate School of Natural Science and Technology, Okayama University, Okayama 700-8530, Japan*
Takanori Wakita − *Graduate School of Natural Science and Technology, Okayama University, Okayama 700-8530, Japan; Research Institute for Interdisciplinary Science, Okayama University, Okayama 700-8530, Japan*
Takayoshi Yokoya − *Graduate School of Natural Science and Technology, Okayama University, Okayama 700-8530, Japan; Research Institute for Interdisciplinary Science, Okayama University, Okayama 700-8530, Japan;* orcid.org/0000-0002-1251-2826
Aichi Yamashita − *Department of Physics, Tokyo Metropolitan University, Hachioji, Tokyo 192-0397, Japan*
Yosuke Goto − *National Institute of Advanced Industrial Science and Technology (AIST), Tsukuba, Ibaraki 305-8568, Japan;* orcid.org/0000-0002-2913-2897
Yoshihiko Takano − *International Center for Materials Nanoarchitectonics (MANA), National Institute for Materials Science, Tsukuba, Ibaraki 305-0047, Japan*
Akira Miura − *Faculty of Engineering, Hokkaido University, Sapporo, Hokkaido 060-0813, Japan;* orcid.org/0000-0003-0388-9696

Complete contact information is available at:
https://pubs.acs.org/10.1021/acsomega.2c08289

Notes

The authors declare no competing financial interest.

■ ACKNOWLEDGMENTS

This work was partly supported by the Grant-in-Aid for Scientific Research (KAKENHI) (nos. 18KK0076, 21H00151, JP20K20522, and JP20H05882), JST-CREST (no. JPMJCR20Q4), and Tokyo Metropolitan Government Advanced Research (no. H31-1). The X-ray photoelectron spectroscopy experiment at SPring-8 was performed under the proposal number 2022A1697.

■ REFERENCES

(1) Lim, Y. S.; Jeong, J.; Kim, J. Y.; Ko, M. J.; Kim, H.; Kim, B.; Jeong, U.; Lee, D.-K. Binder-Free Cu-In Alloy Nanoparticles Precursor and Their Phase Transformation to Chalcogenides for Solar Cell Applications. *J. Phys. Chem. C* **2013**, *117*, 11930−11940.
(2) Yang, J.; Yan, Y.; Wang, Y. X.; Yang, G. Improved thermoelectric performance of CuGaTe2 with convergence of band valleys: a first-principles study. *RSC Adv.* **2014**, *4*, 28714−28720.
(3) Sharma, S.; Verma, A. S.; Jindal, V. K. Ab initio studies of structural, electronic, optical, elastic and thermal properties of silver gallium dichalcogenides (AgGaX2: X=S, Se, Te). *Mater. Res. Bull.* **2014**, *53*, 218−233.
(4) Ullah, S.; Din, H. U.; Murtaza, G.; Ouahrani, T.; Khenata, R.; Naeemullah; Bin Omran, S. B. Structural, electronic and optical properties of AgXY 2 (X = Al, Ga, In and Y = S, Se, Te). *J. Alloys Compd.* **2014**, *617*, 575−583.
(5) Sun, M.; Chen, M.; Li, J.; Hou, J.; Xu, F.; Xu, L.; Zeng, R. Enhanced visible light-driven activity of TiO2 nanotube array photoanode co-sensitized by "green" AgInS2 photosensitizer and In2S3 buffer layer. *Electrochim. Acta* **2018**, *269*, 429−440.
(6) Uematsu, T.; Doi, T.; Torimoto, T.; Kuwabata, S. Preparation of Luminescent AgInS2−AgGaS2 Solid Solution Nanoparticles and Their Optical Properties. *J. Phys. Chem. Lett.* **2010**, *1*, 3283−3287.
(7) Su, D.; Wang, L.; Li, M.; Mei, S.; Wei, X.; Dai, H.; Hu, Z.; Xie, F.; Guo, R. Highly luminescent water-soluble AgInS2/ZnS quantum dots-hydrogel composites for warm white LEDs. *J. Alloys Compd.* **2020**, *824*, 153896.
(8) Torimoto, T.; Tada, M.; Dai, M.; Kameyama, T.; Suzuki, S.; Kuwabata, S. Tunable Photoelectrochemical Properties of Chalcopyrite AgInS2 Nanoparticles Size-Controlled with a Photoetching Technique. *J. Phys. Chem. Lett.* **2012**, *116*, 21895−21902.
(9) Gherouel, D.; Gaied, I.; Amlouk, M. Effect of heat treatment in air on physical properties of AgInS2 sprayed thin films. *J. Alloys Compd.* **2013**, *566*, 147−155.
(10) Zhang, W.; Li, D.; Chen, Z.; Sun, M.; Li, W.; Lin, Q.; Fu, X. Microwave hydrothermal synthesis of AgInS2 with visible light photocatalytic activity. *Mater. Res. Bull.* **2011**, *46*, 975−982.
(11) Wang, D.; Zheng, W.; Hao, C.; Peng, Q.; Li, Y. General synthesis of I-III-VI2 ternary semiconductor nanocrystals. *Chem. Commun.* **2008**, *2008*, 2556−2558.
(12) Dongho Nguimdo, G. M.; Manyali, G. S.; Abdusalam, M.; Joubert, D. P. Structural stability and electronic properties of $AgInS_2$ under pressure. *Eur. Phys. J. B* **2016**, *89*, 90.
(13) Liu, J.; Chen, S.; Liu, Q.; Zhu, Y.; Lu, Y. Density functional theory study on electronic and photocatalytic properties of orthorhombic $AgInS_2$. *Comput. Mater. Sci.* **2014**, *91*, 159−164.
(14) Liu, J.; Hua, E. Electronic structure and absolute band edge position of tetragonal $AgInS_2$ photocatalyst: A hybrid density functional study. *Mater. Sci. Semicond. Process.* **2015**, *40*, 446−452.
(15) Fang, L.; Wang, Y.; Zou, P. Y.; Tang, L.; Xu, Z.; Chen, H.; Dong, C.; Shan, L.; Wen, H. H. Fabrication and superconductivity of Na_xTaS_2 crystals. *Phys. Rev. B* **2005**, *72*, 014534.
(16) Morosan, E.; Zandbergen, H. W.; Dennis, S.; Bos, J. W. G.; Onose, Y.; Klimczuk, T.; Ramirez, A. P.; Ong, N. P.; Cava, R. J. Superconductivity in CuxTiSe2. *Nat. Phys.* **2006**, *2*, 544−550.
(17) Ryu, G. Superconductivity in Cu-Intercalated CdI2-Type PdTe2. *J. Supercond. Novel Magn.* **2015**, *28*, 3275−3280.
(18) Chen, D. Y.; Wu, Y.; Jin, L.; Li, Y.; Wang, X.; Duan, J. X.; Han, J.; Li, X.; Long, Y. Z.; Zhang, X.; Chen, D.; Teng, B. Superconducting properties in a candidate topological nodal line semimetal SnTaS 2 with a centrosymmetric crystal structure. *Phys. Rev. B* **2019**, *100*, 064516.
(19) Matsumoto, R.; Hou, Z.; Nagao, M.; Adachi, S.; Hara, H.; Tanaka, H.; Nakamura, K.; Murakami, R.; Yamamoto, S.; Takeya, H.; Irifune, T.; Terakura, K.; Takano, Y. Data-driven exploration of new pressure-induced superconductivity in PbBi2Te4. *Sci. Technol. Adv. Mater.* **2018**, *19*, 909−916.
(20) Matsumoto, R.; Hou, Z.; Hara, H.; Adachi, S.; Takeya, H.; Irifune, T.; Terakura, K.; Takano, Y. Two pressure-induced superconducting transitions in SnBi2Se4 explored by data-driven materials search: new approach to developing novel functional materials including thermoelectric and superconducting materials. *Appl. Phys. Express* **2018**, *11*, 093101.
(21) Kawaguchi, S.; Takemoto, M.; Osaka, K.; Nishibori, E.; Moriyoshi, C.; Kubota, Y.; Kuroiwa, Y.; Sugimoto, K. High-throughput powder diffraction measurement system consisting of multiple MYTHEN detectors at beamline BL02B2 of SPring-8. *Rev. Sci. Instrum.* **2017**, *88*, 085111.
(22) Petříček, V.; Dušek, M.; Palatinus, L. Crystallographic Computing System JANA2006: General features. *Z. Kristallogr.—Cryst. Mater.* **2014**, *229*, 345−352.

(23) Momma, K.; Izumi, F. VESTA: a three-dimensional visualization system for electronic and structural analysis. *J. Appl. Crystallogr.* **2008**, *41*, 653−658.

(24) Blaha, P.; Schwarz, K.; Tran, F.; Laskowski, R.; Madsen, G.; Marks, L. D. WIEN2k: An APW+lo program for calculating the properties of solids. *J. Chem. Phys.* **2020**, *152*, 074101.

(25) Perdew, J. P.; Burke, K.; Ernzerhof, M. Generalized Gradient Approximation Made Simple. *Phys. Rev. Lett.* **1996**, *77*, 3865−3868.

(26) Matsumoto, R.; Irifune, T.; Tanaka, M.; Takeya, H.; Takano, Y. Diamond anvil cell using metallic diamond electrodes. *Jpn. J. Appl. Phys.* **2017**, *56*, 05FC01.

(27) Jeong, S.; Yoon, H. C.; Han, N. S.; Oh, J. H.; Park, S. M.; Min, B. K.; Do, Y. R.; Song, J. K. Band-Gap States of AgIn5S8 and ZnS-AgIn5S8 Nanoparticles. *J. Phys. Chem. C* **2017**, *121*, 3149−3155.

(28) Shannon, R. D. Revised effective ionic radii and systematic studies of interatomic distances in halides and chalcogenides. *Acta Crystallogr.* **1976**, *32*, 751−767.

https://doi.org/10.1021/acsomega.2c08289
ACS Omega 2023, 8, 11288−11292